Direct-Inverse Method for Airfoils at High Angles of Attack

Leland A. Carlson*
Texas A&M University, College Station, Texas

Presented here is a direct-inverse technique and computer program called TAMSEP that can be used for the analysis of the flow about airfoils at subsonic and low-transonic freestream velocities. The method is based upon a direct-inverse nonconservative full potential inviscid method, a Thwaites laminar boundary-layer technique, and the Barnwell turbulent momentum integral scheme and is formulated using Cartesian coordinates. Since the method utilizes inverse boundary conditions in regions of separated flow, it is suitable for predicting the flowfield about airfoils having trailing-edge separated flow under high-lift conditions. Comparisons with experimental data indicate that the method should be a useful tool for applied aerodynamic analyses.

Nomenclature

a = isentropic speed of sound
c_3^* = boundary-layer coefficient in separated pressure correlation
C_p = pressure coefficient
M = Mach number
q = velocity
U,V = velocity component in the x or y direction, respectively
U_e = transformed velocity at boundary-layer edge
u = velocity in the boundary layer
u^*,u_β = law of the wall and law of the wake velocity parameters
x,y = Cartesian coordinates
α = angle of attack
γ = ratio of specific heats, assumed to 1.4
Γ = circulation
δ = boundary-layer thickness
θ = polar coordinate
ξ,η = computational coordinates
Φ = potential function
ϕ = perturbation potential

Subscripts

∞ = freestream condition
b = body
e = boundary-layer edge
i,j = grid location
LE = leading edge
TE = trailing edge
ξ,η,x,y = differentiation

Introduction

OVER the past decade, several finite-difference potential flow methods[1-3] have been developed and successfully used for the design and analysis of subsonic and transonic airfoils at and near cruise conditions. However, in the analysis of high-performance airfoils, aerodynamicists also want to be able to predict airfoil pressure distributions and aerodynamic coefficients at high-lift, high-angle-of-attack conditions. Since such situations are frequently characterized by regions of separated flow on the upper surface and are dominated by strong viscous interaction effects, inviscid methods alone are not applicable. Furthermore, subsonic transonic analysis methods[3,4] that couple inviscid and boundary-layer solutions typically include only the effects of weak viscous interactions and generally fail to give accurate results when separated flow exists on the upper surface.

However, it has been demonstrated[5-8] that the direct-inverse technique coupled to a suitable boundary-layer method can be successfully applied to low-speed flows about airfoils having massive separation. In addition, Barnwell,[9] Dvorak and Choi,[10] and Taverna[11] have developed similar methods for transonic flows. However, Barnwell's method is limited in application in that it utilizes for its inviscid solver the transonic small-perturbation equation. Further, Refs. 9 and 11 include only the effects of viscous interaction due to a turbulent boundary layer. On most airfoils, particularly on the lower surface at high angles of attack, extensive regions of laminar flow exist.

This paper describes a flow model and computer program, called TAMSEP, which can be used to predict the flowfield about a single-element transonic airfoil at high-angle-of-attack, high-lift conditions with trailing-edge separation. Since the method is based upon the TRANDES[4] and TRANSEP[6] codes, it can also be used for subsonic/transonic analyses not involving separation.

Method of Approach

The present approach is based upon the direct-inverse method developed in the TRANDES and TRANSEP programs and the ability of this method to use either the displacement surface (airfoil ordinate plus displacement thickness) or pressure as the airfoil boundary condition. For the high-angle-of-attack case, the airfoil lower surface experiences only weak viscous interaction and frequently has a long laminar run before its transition to fully turbulent flow. Thus, the present model includes an initial laminar boundary-layer calculation in its viscous interaction section. On the upper surface, the boundary layer is also initially laminar, but quickly becomes turbulent in character; this transition is followed in many cases by boundary-layer separation and a separated zone that can extend over a significant portion of the airfoil surface. In the present model, this separated region is treated inversely in that the pressure distribution along the effective displacement surface streamline is determined iteratively as part of the solution and is used as the airfoil boundary condition. Consequently, the present method has been modeled as shown in Fig. 1.

To obtain the inviscid portion of the flowfield, the full potential equation for two-dimensional compressible flow is

Presented as Paper 86-0245 at the AIAA 24th Aerospace Sciences Meeting, Reno, NV, Jan. 6-9, 1986; received March 7, 1986; revision received Oct. 7, 1986.

*Professor of Aerospace Engineering. Associate Fellow AIAA.

used in nonconservative form as

$$(a^2-\Phi_x^2)\Phi_{xx}-2\Phi_x\Phi_y\Phi_{xy}+(a^2-\Phi_y^2)\Phi_{yy}=0 \quad (1)$$

where the subscripts denote partial differentiation. By defining a perturbation potential ϕ such that

$$\Phi=xq_\infty\cos\alpha+yq_\infty\sin\alpha+yq_\infty\phi \quad (2)$$

where the velocity components are given by

$$U=\Phi_x=q_\infty(\cos\alpha+\phi_x)$$

$$v=\Phi_y=q_\infty(\sin+\phi_y) \quad (3)$$

the governing equation in terms of the perturbation potential can be written as

$$(a^2-U^2)\phi_{xx}-2UV\phi_{xy}+(a^2-V^2)\phi_{yy}=0 \quad (4)$$

with

$$a^2=a_\infty^2-[(\gamma-1)/2](U^2+V^2-q_\infty^2) \quad (5)$$

The nonconservative form of the potential equation was selected for the present problem because for two-dimensional flows results obtained with it agree better with Euler solutions than those obtained using the fully conservative form of the equation.[12] In addition, the conservative formulation appears to break down in two-dimensional cases shortly after the onset of supercritical flow.[13]

In the present model, Eqs. (3-5) are finite differenced using a rotated difference scheme and solved iteratively using column relaxation in a stretched Cartesian grid that maps the infinite domain to a finite computational box. The appropriate boundary condition at infinity as

$$\phi=-\frac{\Gamma}{2\pi}\tan^{-1}[\sqrt{1-M_\infty^2}(\theta-\alpha)] \quad (6)$$

where θ is the polar angle, and Γ the circulation determined by the change in potential across the Kutta-Joukowski cut at the trailing edge of the airfoil.

Likewise, the appropriate airfoil boundary condition in the direct regions (regions without separation having only weak viscous interaction) is the flow tangency condition given by the ordinates of the airfoil displacement surface, i.e.,

$$\left(\frac{dy}{dx}\right)_b=\left(\frac{V}{U}\right)_b=\frac{\sin\alpha+\phi_{yb}}{\cos\alpha+\phi_{xb}} \quad (7)$$

In the inverse or separated flow region, the pressure distribution along the effective displacement surface streamline is considered to be specified and is used as the boundary condition. As shown in Ref. 2, this approach leads to a derivative boundary condition for the inverse region of the form

$$\phi_{xb}=-\cos\alpha+\left(\frac{1}{1+(V^2/U^2)_b}\times\left\{1-\left[\left(1+\frac{\gamma M_\infty^2 C_{pb}}{2}\right)^{(\gamma-1)/\gamma}-1\right]\frac{2}{(\gamma-1)M_\infty^2}\right\}\right)^{1/2} \quad (8)$$

Complete details concerning the finite-difference scheme, the stretched Cartesian grid system, and the treatment of the boundary conditions are given in Refs. 1, 2, and 4.

To include viscous effects, the basic approach is to calculate a boundary-layer displacement thickness for the weak interaction regions and to use it to correct the location of the displacement surface (i.e., airfoil ordinate plus displacement thickness). For the strongly interacting separated zone on the upper surface, the pressure is determined from the interaction solution and the location of the displacement surface is computed by integrating the surface tangency condition [Eq. (7)] with the initial conditions

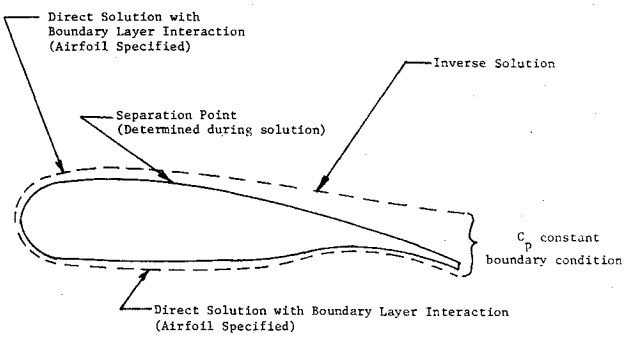

Fig. 1 Problem formulation.

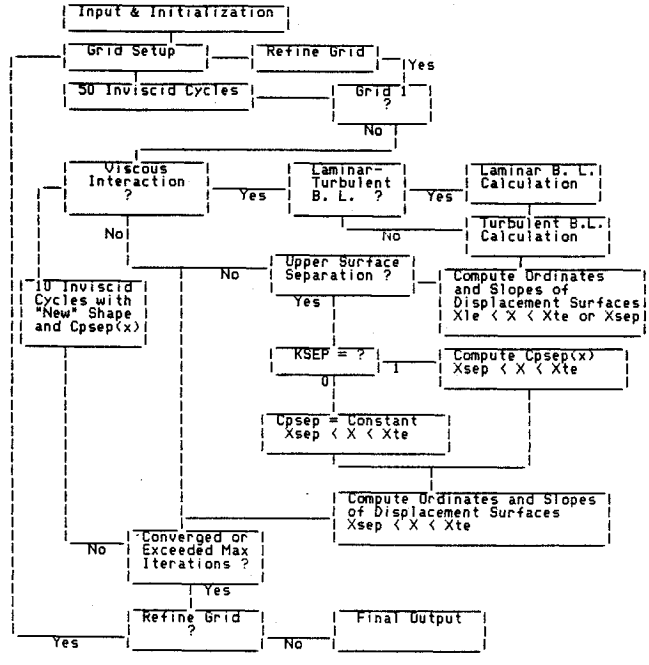

Fig. 2 Iteration and interaction procedure used in TAMSEP.

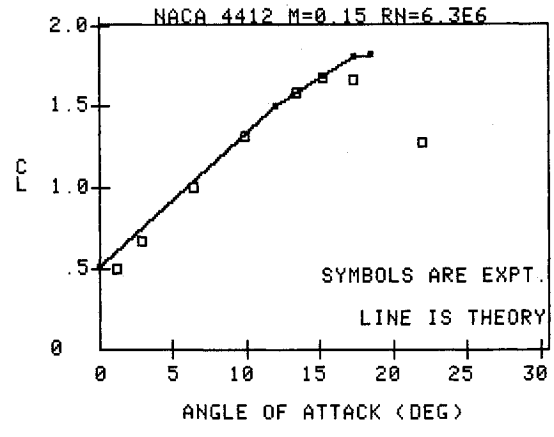

Fig. 3 Comparison of predicted lift coefficient with experimental data, NACA 4412 case.

specified by the displacement surface ordinates at the separation point (the interface between the two regions). The location and slopes of the displacement surfaces are updated regularly throughout the iterative solution.

In the present method, the laminar portion of the boundary layer is computed using a compressible Thwaites method similar to that used previously in TRANSEP.[6] The transition location is determined from a Granville-type correlation[14] based upon the difference between the local momentum thickness Reynolds number and the value at the laminar instability point combined with the pressure gradient history. Sometimes, particularly on the upper surface at high angles of attack, laminar separation is predicted upstream of the transition point. In these cases, the local momentum thickness Reynolds number is compared to an empirical correlation in order to determine if the laminar bubble is long or short. If the bubble is short, its length is assumed equal to the local Δx grid spacing and the turbulent flow computation is initiated at the next downstream grid point. If the estimate indicates that the bubble is long, the calculation proceeds, but a warning is printed to indicate that the results are probably in error.

After transition, the turbulent boundary layer is computed using the simplified Kuhn and Nielsen (SKAN) method as developed by Barnwell.[9] This method was selected because it is efficient and reliable and also yields excellent predictions of displacement thicknesses and separation point location. The SKAN turbulent boundary-layer method solves the integral forms of the momentum and moment of momentum equations and the derivative of the Coles' law of the wall/law of the wake relationship as applied at the boundary-layer edge. After considerable effort,[9] these equations can be transformed into a set of simultaneous ordinary differential equations, i.e.,

$$a_{i1}\frac{du^*}{dx}+a_{i2}\frac{du_\beta}{dx}+a_{i3}\frac{d\delta}{dx}=b_1\frac{dU_e}{du_e}\frac{du_e}{dx}+\frac{a_e}{a_\infty}c_i \qquad i=1,2,3 \qquad (9)$$

which can be solved for the wall friction velocity u^*, the wake parameter u_β, and the boundary-layer thickness δ using a second-order predictor-corrector technique. The remaining quantities of interest (such as the displacement and momentum thicknesses) are then determined from these variables. The numerical integration is terminated at the separation point where the wall friction velocity u^* vanishes.

The method uses a two-layer eddy-viscosity model, which ignores the viscous sublayer terms, consisting of an inner-layer Prandtl mixing length model and an outer-layer Clauser model; and the intermittency factor as well as several density ratios appearing in the fundamental equations are approximated. In addition, the method assumes an adiabatic wall.

Thus, on the lower surface the flow is computed using direct boundary conditions (airfoil specified) including the effects of weak viscous interaction. On the upper surface, the flowfield is also computed directly with viscous interaction up to the separation point, which is determined as part of the boundary-layer solution. Downstream of separation, inverse boundary conditions are utilized and the pressure must be specified. However, if the skin friction at the wall is assumed to be zero in the separated zone, the SKAN formulation can be used to obtain a closed-form solution for the velocity, and hence the pressure, at the outer edge of the separated zone. While this assumption will not be true in all cases, it has been utilized in the present formulation and the resultant analytic expressions for the velocity and pressure are

$$\frac{u_e}{q_\infty}=\frac{0.833c_3^*[\cos\alpha(x_{TE}-x_{sep})+\phi_{TE}-\phi_{sep}]}{\{[1+c_3^*(x_{TE}-x_{sep})]^{5/6}-1\}[1+c_3^*(x-x_{sep})]^{1/2}} \qquad (10)$$

$$C_p=\frac{2}{\gamma M_\infty^2}\left\{\left[1+\frac{\gamma-1}{2}M_\infty^2\left(1-\frac{u_e^2}{q_\infty^2}\right)\right]^{\gamma/(\gamma-1)}-1\right\} \qquad (11)$$

As can be seen, the separated pressure depends upon the flowfield solution via the inviscid perturbation potentials at the separation point and the trailing edge, the size of the separated zone, and, through c_3^*, the boundary-layer solution at the separation point. In addition, this closed-form solution predicts a variable pressure distribution for the separated region. At low freestream Mach numbers, this variation is extremely small and is essentially constant. However, at freestream Mach numbers of 0.3 and above, the variation becomes significant and influences the resultant flowfield solution. This trend and separated pressure variation is in accord with experimental observations and is a significant improvement over previous methods that assumed constant pressure in the separated zone regardless of flow conditions. However, since at low speeds the separated pressure is essentially constant and the complexity introduced by Eqs. (10) and (11) may not be warranted, the present method contains the option of either using a constant pressure in the separated region or the variable distribution determined by the closed-form solution given above.

In principle, the separated region and the wake should be accurately modeled with respect to physical phenomena and internal details; this approach has been taken by other investigators.[10,15,16] In the present model, however, the wake region contains very few computational points since the coordinate system rapidly stretches to infinity. Thus, the wake is assumed to be inviscid with a constant-pressure trailing edge formed by the upper and lower displacement surfaces. Fortunately, extensive numerical experiments with the present and previous[7] models indicate that the pressure distribution and aerodynamic coefficients are primarily dependent upon obtaining accurate predictions for the location of the separation point and magnitude and variation of the separated pressure. Apparently, at least for angles of attack up to the initial stall break, the details of the wake region are of secondary importance. However, for very high angles of attack characterized by leading-edge separation and large possibly unsteady wakes, a detailed wake model would be needed. Nevertheless, since the present method obtains the separation point location directly from the solution for the wall friction velocity u^* and the pressure variation from a solution that couples the inviscid and viscous parts, it should yield reasonable engineering results for many cases of interest.

Interaction and Iteration Procedure

The iteration and interaction procedure used in TAMSEP is similar to that used in the low-speed program TRANSEP[6] and is outlined in schematic form in Fig. 2. After appropriate initialization and grid setup, 50 inviscid interactive cycles are normally computed on a very coarse grid with a default size of 13×7. This limited number of cycles serves to rapidly create an approximate starting solution for succeeding grids. The grid is then halved and the solution interpolated onto a new grid, which has a default size of 25×13. The method then performs 50 inviscid iterative cycles before considering any type of viscous interaction. Experience has shown that it is important to perform a limited number of inviscid cycles at the beginning of each new grid in order to eliminate any "problems" introduced by grid halving and interpolation. If viscous interaction is desired, the program then checks to see if an initial laminar boundary layer is to be included or if the viscous calculations are to be for a turbulent boundary layer with user specified transition points.

Upon completing the boundary-layer computations for the current flowfield solution, the program calculates the ordinates and slopes of the upper and lower displacement surfaces. Since it involves only weak viscous interaction, the lower-surface computations are from the leading edge or the

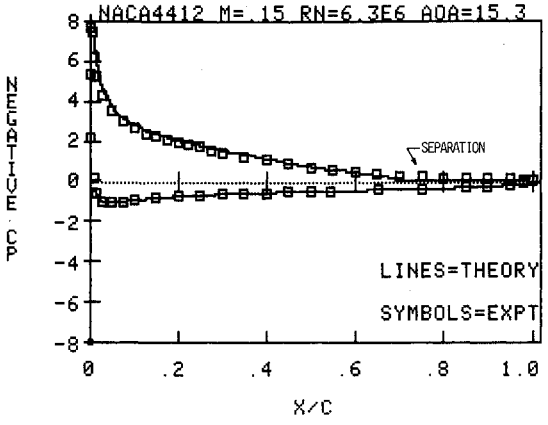

Fig. 4 Comparison of theoretical pressure distribution with experimental data, NACA 4412 case.

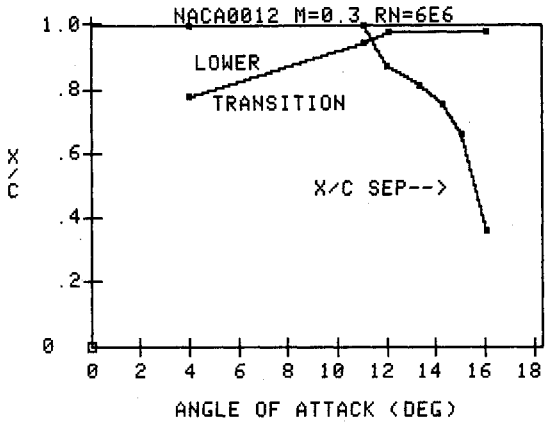

Fig. 5 Lower-surface transition and upper-surface separation locations, NACA 0012 case.

lower-surface stagnation point, whichever is further aft, to the trailing edge. However, on the upper surface, they are only from the leading edge to the separation point or to the trailing edge, whichever is less. This process involves smoothing of the displacement thickness values, properly adding them to the airfoil ordinates, and spline fitting the resulting points.

The procedure next depends upon whether or not separation has been detected on the upper surface. If separation does not exist prior to the last grid point on the airfoil upper surface, additional inviscid cycles are performed before returning to the viscous interaction loop. However, if separation is predicted, the method must determine the pressure distribution and the location of the displacement surface in the separated zone. If desired, the pressure can be assumed constant in the separated zone and computed by

$$C_{p,\text{sep}} = \frac{-2(\phi_{\text{TE}} - \phi_{\text{sep}})}{x_{\text{TE}} - x_{\text{sep}}} \tag{12}$$

While this expression is a small-perturbation approximation for $C_{p,\text{sep}}$, its usage has been found to be accurate and adequate for low-speed incompressible flows. At freestream Mach numbers of 0.3 and higher, however, the variable separated pressure distribution determined by Eqs. (10) and (11) should be used. Note that both approaches determine the separated zone pressure, which depends upon the current solution, by conditions at both the separation point and at the trailing edge and not just on conditions in the vicinity of separation.

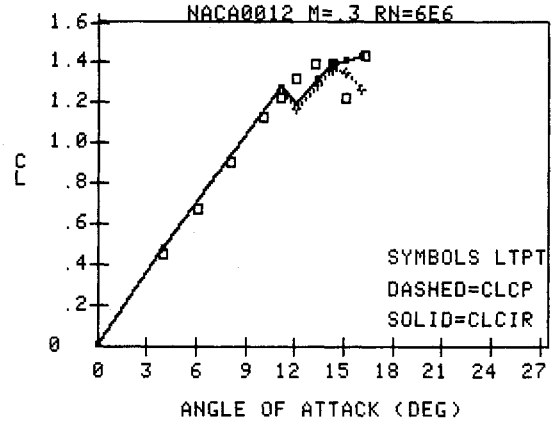

Fig. 6 Comparison of predicted lift coefficient with experimental data, NACA 0012, Mach = 0.3 case.

When separation exists, the previous method of locating the upper displacement surface by adding the computed displacement thicknesses to the original airfoil ordinates is inappropriate, since the predicted displacement thickness values are probably inaccurate in separated regions. Instead, the present approach is to solve, using the current potential flow solution, the differential equation given by Eq. (7) for the y ordinates of the separated displacement surface as a function of x. Based upon previous studies,[2,6] Eq. (7) is solved using the Runge-Kutta method of order four with the displacement surface ordinate at the separation point as the initial condition. In the process of solving this equation, $\phi_{\xi b}$ and $\phi_{\eta b}$ must be evaluated by finite differences. While several formulations are possible,[2] numerical studies indicate that accurate displacement surfaces are obtained using

$$\phi_{\eta b} = \frac{-3\phi_{i,j-1} + 4\phi_{ij} - \phi_{i,j+1}}{2\Delta\eta} + (\eta_b - \eta_{j-1})\frac{\phi_{i,j-1} - 2\phi_{ij} + \phi_{i,j+1}}{\Delta\eta^2} \tag{13a}$$

$$\phi_{\xi b} = \frac{\phi_{i+1,j-1} - \phi_{i-1,j-1}}{2\Delta\xi} + (\eta_b - \eta_{j-1})\frac{\phi_{i+1,j}\phi_{i+1,j-1}\phi_{i-1,j} + \phi_{i-1,j-1}}{2\Delta\xi\Delta\eta} \tag{13b}$$

In Eqs. (13), the point $(i,j-1)$ is the first ghost point below the displacement surface. Its value is determined as part of the inverse pressure boundary condition. Since the present process is iterative and the potential solution uses the separated distribution as an inverse boundary condition, the solution of Eqs. (7) and (13) should yield upon convergence a separated zone displacement surface or free streamline that is compatible with the pressure distribution and potential flow solution.

At this point in the iteration interaction procedure, a check is made to see if the solution has converged or if the maximum number of iterations for a given grid size has been exceeded. If neither is true, 10 more inviscid cycles with the new displacement surfaces and separated pressure distribution are performed prior to repeating the viscous interaction loop. If, however, either condition is satisfied and the finest grid specified by the user has not been used, the grid is refined and the entire process shown in Fig. 2 is repeated. If the last grid solution has been obtained, then a final output is printed and the solution is finished.

It should be noted that the calculations on a given grid are stopped and assumed to be converged when the maximum perturbation potential change is less than some user-specified

value. However, when separation is present, it is usual for the calculations on each grid to be terminated due to the number of iterative cycles exceeding a maximum user-specified value (particularly on computers that retain only seven significant digits). In those cases, the existence or degree of convergence can be determined by examining the variation in the number of supersonic points, the location of separation, and the trailing-edge ordinate of the upper displacement surface. If they stabilize prior to the end of the computation on a given grid, then the results can be assumed to be converged. Normally, it is sufficient to perform 800 cycles on the coarse grid (25×13), 400 on the medium grid (49×25), and 400 on the fine grid (97×49), although occasionally more may be needed. In nonoverlay mode the code requires less than 320×10^3 bytes and it obtains a solution on an Amdahl 470/V8 at a rate of about 15,000 points/s.

In determining convergence, it should be remembered that the present method is supposed to obtain a steady-state solution. At angles of attack above maximum lift, the actual flowfield about an airfoil is usually unsteady[17,18] and the details of the wake become important. In those cases, the present method probably will not converge and may enter some type of oscillatory behavior that appears to represent an unsteady flow pattern. However, the present method is not "time accurate" and such results should be viewed only as indicative of the presence of significant unsteady phenomena.

Typical Results

In the development of the present method, results have been obtained for NACA 4412 and 0012 airfoils for freestream Mach numbers up to 0.6, angles of attack up to 18.5 deg, and Reynolds numbers between 3 and 9×10^6. These conditions were selected not because of limitations in the method, but due to the availability of excellent experimental pressure distribution data in those regions.[19-21] Thus, the results presented here are meant only to be representative.

Figures 3 and 4 compare results obtained with the present method with the low speed experimental data of Pinkerton[21] for a NACA 4412 airfoil at 6.3×10^6 Reynolds number. In Fig. 3, the experimental data have been plotted using the angle-of-attack correction suggested in Ref. 21. As can be seen, the theory predicts slightly larger lift coefficients than the data at the lower angles of attack. Whether this difference is due to an underestimation of the angle-of-attack correction, as suggested in Ref. 22, or a problem in the theoretical model is unknown. In any event, the theory and the data are in excellent agreement between 10 and 15 deg and the present model reasonably predicts the location of maximum lift at an angle of attack of about 16–17 deg. The theoretical model does, however, overpredict slightly (1.8 vs 1.7) the maximum lift coefficient predicted by this 47 year old data.

Figure 4 compares pressure distribution results obtained with the present method with the experimental data at an angle of attack slightly below that corresponding to maximum lift. In this case, the corrected angle of attack was used in the computations and the upper- and lower-surface boundary layers were assumed to be initially laminar, followed by natural transition to turbulent flow. For this high-lift case, the theory predicts that the lower surface remains entirely laminar and that the upper surface transitions at 1% chord followed by separation at 74.9% chord. As can be seen, the predicted pressure distribution is in excellent agreement with the data and the pressure coefficient in the separated zone is slightly negative and constant. Experience indicates that, for low-speed cases, better results are usually obtained using the constant-pressure option for the separated zone. For this case, the theoretical lift coefficient was 1.69, while the experimental value was 1.68. The predicted profile drag coefficient was 0.0200, which is in reasonable agreement with available measurements.[23]

As indicated previously, it is important for this type of method to include the effects of a laminar boundary layer. Figure 5 shows lower surface laminar/turbulent transition point locations predicted by the present method for a NACA 0012 airfoil at Mach 0.3 and 6×10^6 Reynolds number. For these flight conditions, the lower-surface boundary layer is predominantly laminar at low angles of attack; and at angles of attack above 10 deg, it is essentially all laminar. Obviously, a method that includes only a turbulent boundary-layer calculation and/or assumes transition near the leading edge might yield incorrect results for these flight conditions.

Figure 5 also shows for the same conditions the predicted upper-surface separation points determined by the TAMSEP method. Notice that no upper-surface separation is predicted until about 12 deg angle of attack. After that, as the angle of attack increases, the beginning of separation moves forward on the upper surface until more than half of the airfoil experiences separated flow at about 16 deg. For this case, maximum lift occurs around 14 deg.

Figure 6 compares the predicted lift coefficient variation with angle of attack for a NACA 0012 airfoil at the same nominal conditions (i.e., Mach 0.3 and 6×10^6 Reynolds number) with experimental data obtained in the Low Turbulence Pressure Tunnel at NASA Langley.[20] These data were obtained on clean airfoils without the use of trip strips and, thus, the theoretical results were obtained using the laminar natural transition turbulent model. At the lower angles of attack, the agreement is quite good. However, at the onset of trailing-edge separation, around 12 deg, the theoretical lift curve exhibits a "kink" accompanied by a slight decrease in lift coefficient. This "kink" is often observed in the theoretical lift curves when separation is first predicted and is due to the fact that separation is usually first detected on the coarse grid. On that grid, the first point forward of the trailing edge is about 93% chord; and, thus, when separation is first predicted on the coarse grid, the separation point moves forward from the trailing edge to at least the 93% point, with the result that the amount of separation is overpredicted and the lift at that condition is underpredicted. Since the model permits the separation point to move only forward, this effect is maintained throughout all the grids at that angle of attack. However, as the angle of attack is increased, this effect disappears. Thus, at low and medium freestream Mach numbers, the lift coefficients predicted at angles of attack just above the onset of trailing-edge separation are usually slightly low.

However, as can be seen on Fig. 6, the lift coefficients predicted at the higher angles of attack are, at least for this case, in reasonable agreement with the experimental data. Notice that for this case the experimental data indicate an apparent maximum lift around 14 deg followed by a decrease and then an increase. The theoretical lift based upon the calculated circulation predicts a maximum lift coefficient of about 1.40 at 14–16 deg. On the other hand, the theoretical lift based upon integration of the pressure distributions indicates maximum lift at 14 deg, which nominally agrees with experimental data. This slight divergence between the values predicted by circulation and those by pressure integration is, based upon experience, an excellent indication of the maximum lift location at low and medium speeds. The reason for this statement will be evident when the pressure distributions for these cases are discussed.

The predicted variation of drag with lift for this case is compared to experimental data at the higher lift coefficients on Fig. 7. Again, the zig-zag in the theoretical curve corresponds to the similar phenomena on the lift vs angle-of-attack plot and is due to the overprediction of the size of the initial separated zone. Nevertheless, the agreement between the theoretical predictions and experimental values, particularly near maximum lift, is good.

Figure 8 compares pressure distributions obtained with the present method with data obtained in the Low Turbulence Pressure Tunnel at NASA Langley[20] at three different angles

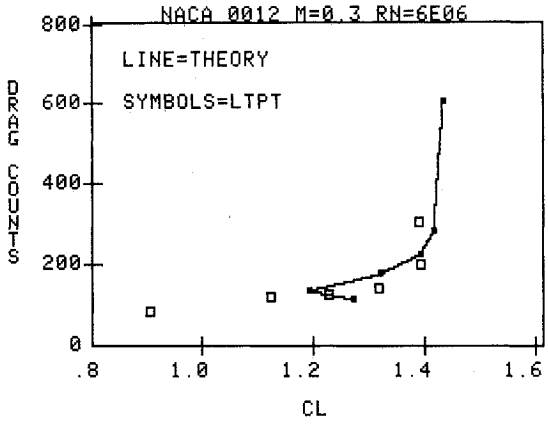

Fig. 7 Comparison of theoretical lift and drag with experimental data, NACA 0012, Mach = 0.3 case.

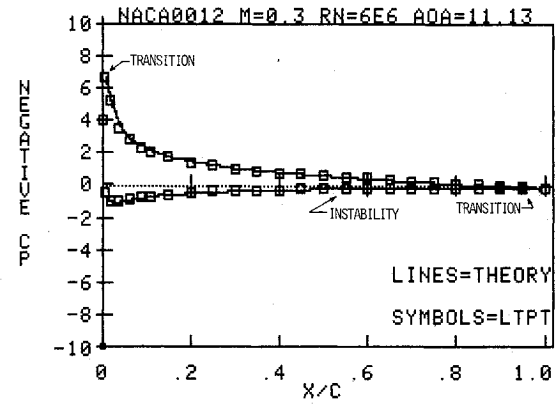

Fig. 8a Theoretical and experimental pressure distribution comparisons, NACA 0012 at 11.13 deg angle of attack.

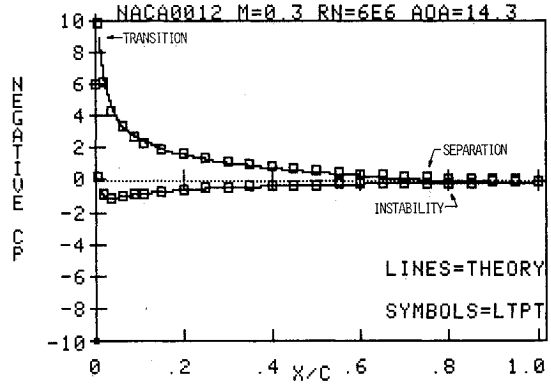

Fig. 8b Theoretical and experimental pressure distribution comparisons, NACA 0012 at 14.3 deg angle of attack.

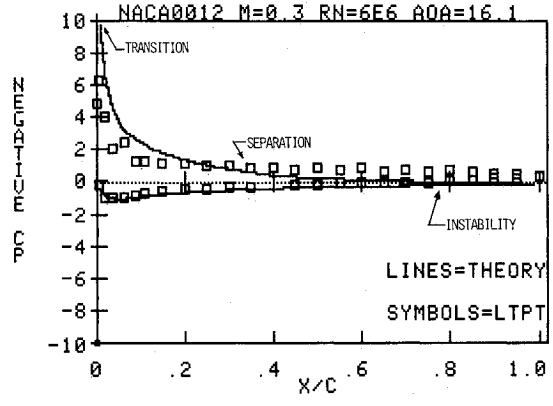

Fig. 8c Theoretical and experimental pressure distribution comparisons, NACA 0012 at 16.1 deg angle of attack.

of attack. The first corresponds to an unseparated flow situation, the second is near maximum lift, and the third is for an angle of attack above the maximum lift condition. Since at medium freestream Mach numbers and higher, evidence[9,19,20] indicates that the pressure variation in a separated zone is not constant, these and subsequent cases were all run using the variable pressure option. As can be seen in Fig. 8a, the theoretical pressure distribution for the unseparated case is in excellent agreement with experimental data. For this case, the theoretical lift and drag coefficients were 1.27 and 0.0116, while the corresponding clean airfoil experimental values were 1.23 and 0.0123.

For the case near maximum lift (Fig. 8b), it should be noted that some supersonic flow exists over the upper surface of the airfoil in a very small region near the leading edge, since the critical C_p for this case is -6.89. In addition, the theoretical method predicts upper surface separation at 74.9% chord and boundary-layer instability on the lower surface at about 80% chord. However, due to the favorable pressure gradient, the lower-surface boundary layer never transitions. For this case, the theoretical lift coefficient of 1.39 coincides with the experimentally measured value and the two pressure distributions exhibit reasonable agreement.

At an angle of attack greater than that corresponding to maximum lift, the flow about an airfoil is typically characterized by a large region of unsteady separated flow and a steady-state solution method such as the present one is not really applicable. Thus, the apparent lack of agreement between the present steady theory and the experimental measurements shown in Fig. 8c is not surprising. Nevertheless, the general pattern of the pressure distribution, including the existence of a large separation zone, is predicted and the predicted lift coefficient of 1.44 based upon circulation is in surprising agreement with the experimentally measured value of 1.437. However, careful examination of the solution indicates that it is not completely converged, that the theoretical lift may be oscillating slightly, and that the lift based upon pressure integration computed at the end of a run using default parameters is only 1.27. Interestingly, results using the thin-layer Navier-Stokes equation[17,18] for a similar case (NACA 0012, Mach 0.3, 1×10^6 Reynolds number, 18 deg angle of attack) indicate a lift coefficient varying with time of 0.65–1.6 with a Strouhal number of 0.1; both of the theoretical and experimental pressure profiles shown in Fig. 8c are representative of those computed at various times in the cycle with the thin-layer Navier-Stokes model. Thus, the present theoretical result is representative of the type of pressure distribution and lift that might exist for this condition.

Another interesting feature associated with the results shown in Fig. 8c is that the drag coefficient predicted using the method of Ref. 6 was 0.0604, while that predicted using the method of Ref. 9 was 0.1190. Normally, these two values are in good agreement with each other. Apparently, in the present method, when the maximum lift condition is exceeded, the solution becomes oscillatory and not completely converged, the lift computed by pressure integration diverges from and is lower than that from circulation, and the two drag coefficient values differ significantly. It is believed that these three items can be used to determine, for medium Mach numbers, the angle of attack corresponding to maximum lift.

For the same NACA 0012, Mach 0.3, and 6×10^6 number case, Fig. 9 shows the displacement surfaces predicted by the present method for the upper-surface region between 70% chord and the trailing edge at various angles of attack.

Below 11.3 deg, where the flow is unseparated, the displacement thicknesses in the trailing-edge zone are relatively small. However, with the onset of separation at 12.09 deg, the thicknesses begin to increase rapidly and the displacement surfaces take on shapes characteristic of the flow over a stalled airfoil. It should be noticed that, at an angle of attack of 16.12 deg, the displacement surface starts to curve back toward the freestream angle prior to the trailing edge. It is believed that the displacement surfaces shown in this figure have the correct behavior and are an adequate engineering representation of the real flow.

Obviously, it would be desirable for the present method to accurately model transonic flows with and without significant trailing-edge separation. Consequently, predictions obtained with TAMSEP have been compared with data obtained in the NASA 8 ft Transonic Pressure Tunnel by Harris.[19] These data probably represent the best high-lift transonic experimental airfoil data available today and they have been used by many investigators. However, most previous studies have compared results using the tunnel geometric angle-of-attack values and have ignored the known corrections associated with these data. Since such comparisons could lead to erroneous conclusions, the present results were obtained by matching the tunnel Mach and Reynolds numbers and using the corrected angles of attack suggested by Harris.

Figure 10 shows a transonic separated flow result compared with data obtained by Harris.[19] While the pressure distribution shown was obtained using the laminar/turbulent boundary-layer option, indistinguishable results were obtained assuming transition at 6% chord. In the actual experiment, boundary-layer trip strips were located at 5% chord. For this case, the present method predicts upper surface separation at 87% chord and lower-surface transition very near the trailing edge. While the experimental shock location is slightly forward of the theoretical value and while the experimental pressures in the trailing-edge region are slightly lower than those predicted by the theory, the overall agreement is probably acceptable for engineering studies. For this case, the measured normal force coefficient was 0.994, while the predicted list coefficient was 0.981.

A lift vs angle-of-attack curve typical of those predicted by the present method is compared with experimental data in Fig. 11. For this freestream Mach number of 0.5, significant transonic flow accompanied by a strong shock wave is present on the upper surface at angles of attack greater than 6 deg. As can be seen, the theoretical prediction, which was obtained assuming transition at 6% chord, agrees well with the experimental data up to about 7.35 deg. Above that angle of attack, the present method predicts a maximum lift coefficient of 1.09 at 8.24 deg with no trailing-edge separation. At 9.21 deg, the theory predicts a decrease in lift coefficient to 0.982 with upper-surface separation at 87% chord. The experimental data, however, indicate that the maximum lift is 1.02 at 9.21 deg and that the trailing-edge separation probably started at about 7.5 deg. Examination of the theoretical results at 7.35 deg reveals that the local Mach number immediately upstream of the upper-surface shock wave is 1.42. Such a strong shock wave, whose strength increases with angle of attack, should induce a significant shock/boundary-layer interaction that, unfortunately, is not modeled in the present theory and code. Therefore, in this case, the differences between the theoretical results and the

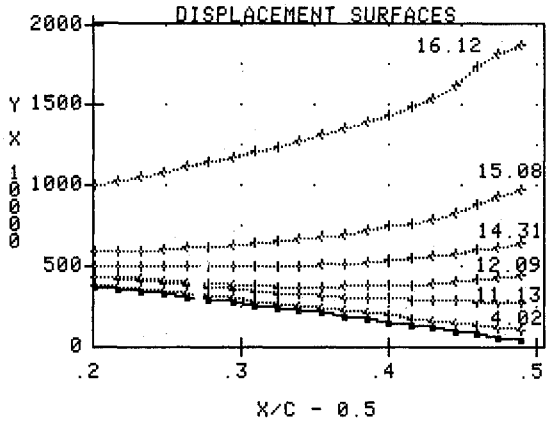

Fig. 9 Predicted displacement surfaces for NACA 0012 at a Mach number of 0.3.

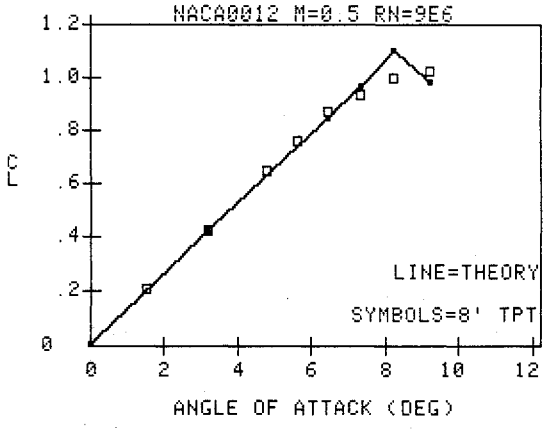

Fig. 11 Comparison of predicted lift coefficient with experimental data, NACA 0012, Mach = 0.5 case.

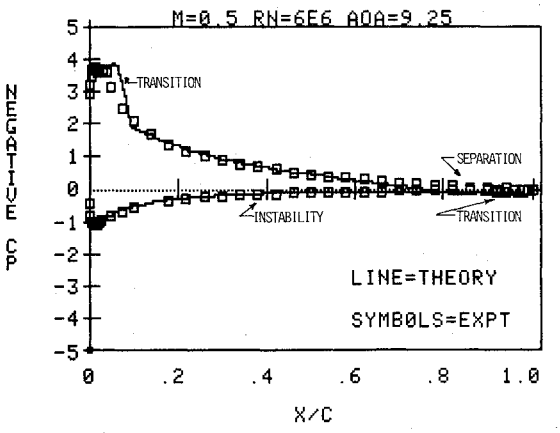

Fig. 10 Theoretical and experimental pressure distribution comparison, NACA 0012 at Mach 0.5.

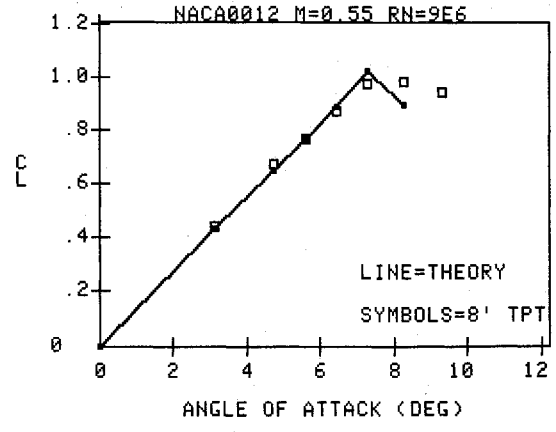

Fig. 12 Comparison of predicted lift coefficient with experimental data, NACA 0012, Mach = 0.55 case.

experimental data near maximum lift are probably due to shock/boundary-layer interaction and its subsequent effect on boundary-layer growth and trailing-edge separation. Nevertheless, the present model does give a reasonable indication of the location and magnitude of the maximum lift coefficient.

A similar lift curve for a freestream Mach number of 0.55 is shown in Fig. 12. As before, the theoretical results were obtained using an all-turbulent boundary layer; in this case, no upper-surface trailing edge separation was detected until an angle of attack of 8.266 deg. The maximum lift coefficient was computed to be 1.02 at 7.29 deg as compared to the experimental values of 0.983 and 8.266 deg. For this case, significant transonic flow existed at all angles of attack above 4.5 deg and by 7.29 deg the Mach number at the upper-surface shock wave had increased to 1.50. At 9.33 deg, a complete solution could not be obtained with the present method. On the medium grid, the upper surface flow separated at 87% chord and, on the fine grid, the separation point moved forward to the shock wave at about 18% chord and the solution failed. Quite obviously, significant shock/boundary-layer interaction exists at these high angles of attack and the decrease in lift or stall is probably due more to shock-induced separation than to the onset of significant trailing-edge separation.

Nevertheless, the present method can be used to estimate reasonably accurately the occurrence of this situation. As can be seen in Fig. 12, the method predicts reasonably well the magnitude of the maximum lift coefficient and is conservative as to the corresponding angle-of-attack location. In addition, by noting the mechanism of code "failure," in this case sudden separation at the shock wave, a user can probably determine the type of stall phenomena present.

Theoretical pressure distribution results are compared with experimental data for a freestream Mach number 0.6 case in Fig. 13. At a corrected angle of attack of 5.59 deg and 3×10^6 Reynolds number, this case is significant for a variety of reasons. First, it is an example of a transonic case with a strong upper-surface shock wave. Second, the flow is unseparated and the data should serve as a good test of the present method for a situation without separation. Finally, this case has also been solved by Anderson et al.[17] using both an Euler boundary-layer method and a thin-layer Navier-Stokes method.

It should be noticed that the present results, like those of Anderson, agree very well with the experimental pressure distribution with respect to the shock location and pressure levels. Also, for this case the experimental lift coefficient was 0.781. The present TAMSEP method predicted 0.809, the Euler boundary-layer method of Anderson yielded 0.804, while his thin-layer Navier-Stokes result was 0.793. Obviously, the present method is capable of yielding excellent results that are in agreement with experimental data and other analytical methods. However, since it is a nonconservative full potential method, it should obtain such results with accurate shock wave locations more easily and faster than other more complicated methods.

Another comparison of lift vs angle of attack is shown in Fig. 14 for the NACA 0012 at a freestream Mach number of 0.6 and a Reynolds number of 9×10^6. As can be seen, the highest theoretical point plotted is at a lift coefficient value of 0.945 and an angle of attack of 6.392 deg. At 7.348 deg, the boundary-layer solution on the medium grid was frozen due to internal problems in the code resulting from shock/boundary-layer interaction; and on the fine grid, the flow separated at the shock wave and a converged solution was not obtained. At 8.371 deg, the flow separated at the upper-surface shock wave on the coarse grid and, again, a converged solution was not obtained. For these cases, computed local Mach numbers in the vicinity of the shock wave were as high as 1.56. Thus, the theory indicates that above 6.392 deg significant shock/boundary-layer interaction probably accompanied by separation exists and that the maximum lift coefficient occurs at that angle of attack. As can be seen in Fig. 14, the magnitude of the predicted maximum lift coefficient is in good agreement with the experimental data, although the angle-of-attack location is again conservative.

Finally, with only minor modifications, the present method can be used to predict the flowfield about an airfoil having a spoiler on the upper surface. Figures 15 and 16 show results obtained for NACA 0012 at a freestream Mach number of 0.6. For these cases, a 15% chord spoiler located

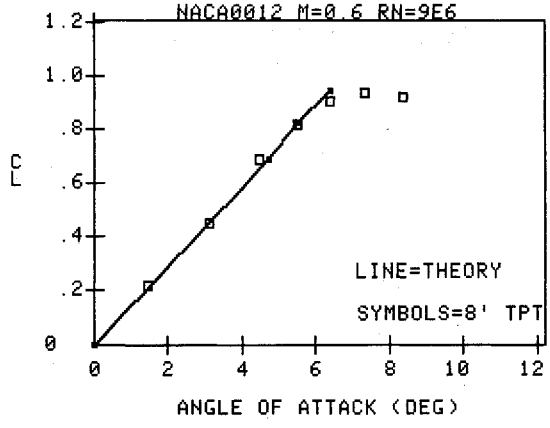

Fig. 14 Comparison of predicted lift coefficient with experimental data, NACA 0012, Mach = 0.6 case.

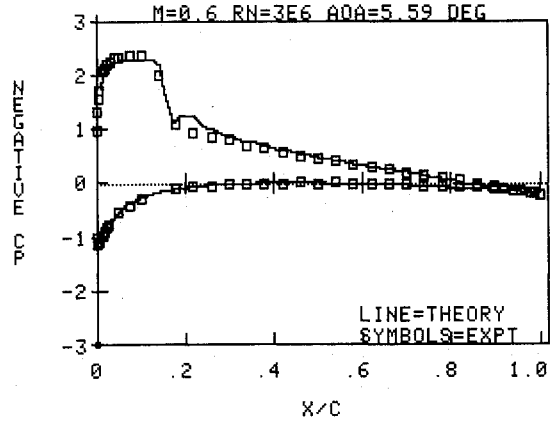

Fig. 13 Theoretical and experimental pressure distribution comparison, NACA 0012 at Mach 0.6.

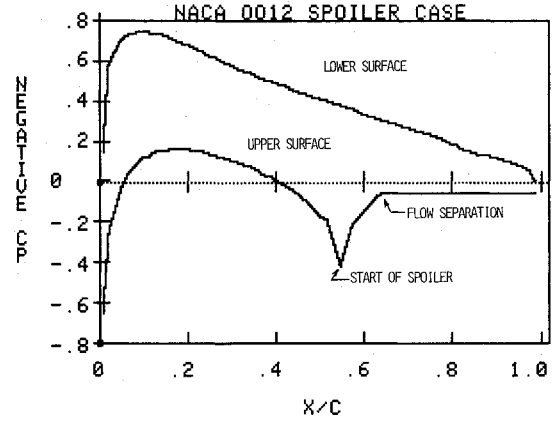

Fig. 15 Theoretical pressure distribution for a spoiler case, Mach = 0.6, $\alpha = 0$ deg spoiler at 55% chord, deflection 5 deg.

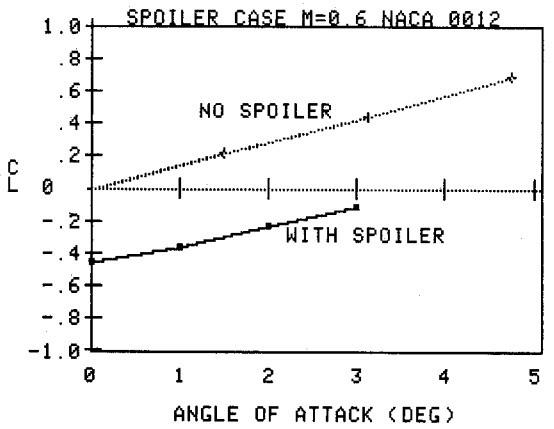

Fig. 16 Comparison of predicted lift coefficient with and without spoiler deflection.

at 55% chord was deflected upward 5 deg. As can be seen in Fig. 15, the upper-surface pressure distribution is significantly changed due to the presence of the spoiler and the flow separates at the trailing edge of the spoiler. As shown in Fig. 16 for several angles of attack, this spoiler effect, as expected, drastically reduces the value of the lift coefficient.

Based upon the results presented in this section, it is believed that the present method and code can be used at low and medium Mach numbers to accurately predict lift and pressure distributions at angles of attack up to that associated with maximum lift. At transonic speeds, the method should give good results for unseparated flows and for flows having trailing-edge separation without significant shock/boundary-layer interaction. Thus, at transonic conditions, the method is probably currently limited, for accurate results, to Reynolds numbers of 3×10^6 and higher and to local upper surface Mach numbers less than 1.4–1.45. In addition, it should yield reasonable estimates for the maximum lift coefficient at transonic speeds, while being conservative as to the corresponding value of angle of attack; and the method should indicate the onset of significant shock/boundary layer-interaction.

Conclusions

A direct-inverse technique based upon a nonconservative full potential inviscid method, a Thwaites laminar boundary-layer technique, and the Barnwell turbulent momentum integral method has been developed. This method is suitable for predicting the subsonic and transonic flowfield about airfoils having trailing-edge separated flow. Extensive comparisons with experimental data indicate that the method should be a useful tool for applied aerodynamic engineering analyses. In addition, it is believed that the range of applicability of the method could be extended significantly by the addition of a shock/boundary-layer interaction model.

Acknowledgment

The work presented in this paper was sponsored by the NASA Langley Research Center under Grant NSG-1174. Copies of the program are available to qualified requestors.

References

[1]Carlson, L. A., "Transonic Airfoil Flowfield Analysis Using Cartesian Coordinates," NASA CR-2577, Aug. 1975.

[2]Carlson, L. A., "Transonic Airfoil Design Using Cartesian Coordinates," NASA CR-2578, April 1976.

[3]Bauer, F., Garabedian, P., Korn, D., and Jameson, A., *Supercritical Wing Sections, Part II,* Springer-Verlag, New York, 1975.

[4]Carlson, L. A., "TRANDES: A Fortran Program for Transonic Airfoil Analysis and Design," NASA CR-2821, June 1977.

[5]Barnwell, R. W., "Two Inviscid Computational Simulations of Separated Flow About Airfoils," AIAA Paper 76-379, July 1976.

[6]Carlson, L. A., "TRANSEP: A Program for High Lift Separated Flow About Airfoils," NASA CR-3376, Dec. 1980.

[7]Carlson, L. A., "A Direct-Inverse Technique for Low Speed High Lift Airfoil Flowfield Analysis," *Computation of Viscous-Inviscid Interactions,* AGARD CP-291, Feb. 1981, pp. 26-1—26-10.

[8]Blascovich, J. D., "Characteristics of Separated Flow Airfoil Analysis Methods," AIAA Paper 84-0048, Jan. 1984.

[9]Barnwell, R. W., "A Potential-Flow/Boundary-Layer Method for Calculating Subsonic and Transonic Airfoil Flow with Trailing Edge Separation," NASA TM-81850, June 1981.

[10]Dvorak, F. A. and Choi, D. H., "Separation Model for Two-Dimensional Airfoils in Transonic Flow," *AIAA Journal,* Vol. 22, Aug. 1984, pp. 1064–1070.

[11]Taverna, F., "Prediction of Subsonic/Transonic Separated Flow about Airfoils," AIAA Paper 85-0205, Jan. 1985.

[12]Rizzi, A., and Viviand, H. (eds.), *Numerical Methods for the Computation of Inviscid Transonic Flows with Shock Waves,* Vieweg, Braunschweig, FRG, 1981.

[13]Salas, M. D., and Gumbert, C. R., "Breakdown of the Conservative Potential Equation," AIAA Paper 85-0367, Jan. 1985.

[14]Schlichting, H., *Boundary Layer Theory,* 6th ed., McGraw-Hill, New York, 1968, p. 479.

[15]Maskew, D. and Dvorak, F. A., "Investigation of Separation Models for the Prediction of $C_{L\max}$," AHS Paper 77-33-01, May 1977.

[16]Henderson, M. L., "A Solution to the 2-D Separated Wake Modeling Problem and its Use to Predict $C_{L\max}$ of Arbitrary Airfoil Sections," AIAA Paper 78-156, Jan. 1978.

[17]Anderson, W. K., Thomas, J. L., and Rumsey, C. L., "Application of Thin-Layer Navier-Stokes Equations Near Maximum Lift," AIAA Paper 78-156, Jan. 1978.

[18]Rumsey, C. L., "Time-Dependent Navier-Stokes Computations of Separated Flows over Airfoils," AIAA Paper 85-1684, July 1985.

[19]Harris, C. D., "Two-Dimensional Aerodynamic Characteristics of the NACA 0012 Airfoil in the Langley 8-Foot Transonic Pressure Tunnel," NASA TM-81927, April 1981.

[20]Ladson, C. L., Private communication.

[21]Pinkerton, R. M., "The Variation with Reynolds Number of Pressure Distribution over an Airfoil Section," NACA Rept. 613, 1938.

[22]Coles, D. and Wadcock, A., "A Flying-Hot-Wire Study of Two-Dimensional Mean Flow Past an NACA 4412 Airfoil at Maximum Lift," AIAA Paper 78-1196, July 1978.

[23]Abbot, I. H. and Von Doenhoft, A. E., *Theory of Wing Sections,* Dover, New York, 1959, p. 489.